





Perpendicular magnetic anisotropy induced by 6*p* atomic layers: Crucial role of interface structural order

Bo-Yao Wang ^{1,*}, Chun-Yao Hsu,¹ Bo-Xiang Liao,¹ Yen-Ling Hsu,¹ Yen-Ming Lai,¹ Ming-Shian Tsai,^{1,2}
Tzu-Hung Chuang ³ and Der-Hsin Wei ³

¹*Department of Physics, National Changhua University of Education, Changhua 500, Taiwan*

²*Institute of Photonics Technologies, National Tsing Hua University, Hsinchu 300, Taiwan*

³*National Synchrotron Radiation Research Center, Hsinchu 300, Taiwan*

 (Received 11 July 2021; revised 27 October 2021; accepted 1 November 2021; published 8 November 2021)

Two-dimensional atomic layers composed of metallic atoms with a high principal quantum number in valence shells are promising materials for applications in state-of-the-art magnetic devices due to the presence of a strong spin-orbit coupling. In this work we experimentally explored the effects of triggering perpendicular magnetic anisotropy (PMA) of ferromagnetic (FM) films by applying a series of 6*p*-Pb, Bi and 4*d*-Pd (reference) atomic layers with high-level atomic orbital and low-level lattice strain. Our research indicates that, compared with Pd atoms, Pb and Bi atoms can produce higher-strength PMA on adjacent FM films through orbital hybridization at the interface. Moreover, we demonstrate that the PMA induced by Pb and Bi atoms is highly sensitive to the ordering degree of the wetting layer which is determined by the interplay of surface free, cohesive, and strain energies within the grown materials; the Pb(Bi) atoms added on the wetting layer can enhance the PMA of the adjacent FM film only when the wetting layer maintains an ordered structure. This work clarifies the critical interface effects of 6*p*-HMs on the FM layer, thus providing important clues to increase control over the spin-orbit interaction engendered by HMs through the interface.

DOI: [10.1103/PhysRevB.104.174407](https://doi.org/10.1103/PhysRevB.104.174407)

I. INTRODUCTION

Two-dimensional atomic layers composed of metallic atoms with high principal quantum numbers in valence shells have attracted considerable research interest not only because their specific structures differ from those of their bulk counterparts but also because they generate high spin-orbit interactions, which are promising for applications in perpendicular-based spin-transfer torque devices [1–6], spin-orbit torque memories [7–13], and even quantum materials [14–20]. In these state-of-the-art magnetic devices, the key spin-orbit coupling effects is expected to be highly related to the structural order or material interface. Despite being highly desirable, experimental investigations of the interplay among the crystal structure, orbital hybridization, and spin-orbit coupling (three crucial, interrelated components) in a model system with well-defined structure, interface, and magnetism have been scarce.

6*p*-Pb and Bi heavy metals (HMs) are stable elements with high-level atomic orbital and large spin-orbit-coupling constants [21]. First-principle calculations indicate that strong orbital hybridization and giant spin-orbit coupling at the HM-FM interfaces can trigger sizable perpendicular magnetic anisotropy (PMA) on adjacent FM films [22–24]. In particular, the Bi/CoFe/MgO structure produces a substantial PMA with a value approximately three times that of the conventional Ta/CoFe/MgO structure [23]. Therefore,

applying 6*p*-HMs could be a possible approach to accomplishing advanced perpendicular-based magnetic devices with high thermal stability. Practically, however, the stability of these theoretically proposed structures is hindered by the considerable lattice mismatch between Pb(Bi) and CoFe films (20%–23%). To examine the key spin-orbit coupling effects of Pb(Bi) atomic layers on magnetism, acquiring a Pb(Bi)/FM system with compatible crystalline structure is crucial, and this requires the minimization of the lattice mismatch between the Pb(Bi) and FM substrate. As detailed in Table I [25,26], the lattice mismatch between Pb(Bi) and the surface layer grown in the *c*(2×2) structure of Cu(001) is reduced to approximately −3.3% (−6.1%). Therefore, Pb(Bi) atomic layers grown on epitaxial magnetic Co/Ni/Cu(001) films [27] could become model systems for experimentally exploring the effects of the 6*p*-HMs on the magnetism as well as the spin-orbit coupling with the adjacent FM films—the phenomena of which remain unclear.

In this work we employed multiple *in situ* techniques to comprehensively investigate the PMA induced in 2-ML Co/15-ML Ni/Cu(001)(Co/Ni/Cu) layers after growth of 6*p*-Pb, Bi and 4*d*-Pd (reference) atomic layers. Our results indicate that Pb(Bi) and Pd atoms grown on Co/Ni films are in layer-plus-island and layer-by-layer modes, respectively. Compared with Pd atoms, Pb and Bi atoms can produce higher strengths of PMA on adjacent Co/Ni films. X-ray measurements verified that PMA originates from the enhancement of the magnetocrystalline anisotropy (MCA) of the interfacial Co layer, which is caused by the orbital hybridization at the interface between 3*d*-Co and 6*p*-Pb(Bi) with very large

*bywang1735@cc.ncue.edu.tw

TABLE I. In-plane lattice constants (a_{\parallel}) of Pd, Pb, Bi, Co, Ni, and Cu (in Å) at {100} surface [25,26], and the lattice mismatch ($\Delta a_{\parallel}/a_{\parallel}$) between these materials and the surface layer grown into the $p(1\times 1)$ or $c(2\times 2)$ structure of Cu(001). The a_{\parallel} of the Bi layer was estimated using the metallic radius of the bulk structure [26].

Elements	Pd	Pb	Bi	Co	Ni	Cu- $p(1\times 1)/c(2\times 2)$
a_{\parallel} at {100} surface	3.88	4.94	4.80	3.52	3.54	3.61/5.10
$\Delta a_{\parallel}/a_{\parallel}$ [$p(1\times 1)$]	7.7%			-2.5%	-1.9%	
$\Delta a_{\parallel}/a_{\parallel}$ [$c(2\times 2)$]		-3.3%	-6.1%			

spin-orbit coupling. We demonstrate further that the PMA induced by Pb and Bi is highly sensitive to the order of the wetting layer which is determined by the interplay of surface free, cohesive, and strain energies within the grown materials; the Pb(Bi) atoms added on the wetting layer can enhance the PMA of the adjacent Co/Ni film only when the wetting layer maintains an ordered structure. Our study clarifies the critical interface effects of $6p$ -HMs on the FM layer, thus offering important clues to increase control over the spin-orbit interaction engendered by HMs through the interface.

II. EXPERIMENT

In this study the growth, crystalline structure, and magnetic properties of a series of Pd, Pb, and Bi/Co/Ni films were investigated *in situ* in a multifunctional ultrahigh-vacuum chamber with a base pressure of 2×10^{-10} Torr. Cu(001) substrates with miscut angles of less than 0.1° were cleaned by applying cycles of 2 keV Ar^{+} ion sputtering and subsequent annealing at 800 K for 5 min to obtain a well-ordered crystalline structure and smooth surface. All films were deposited at room temperature by using thermal evaporation guns with a flux monitor. After a 15 ML Ni film was deposited on Cu(001), the sample was annealed at 430 K for 10 min to improve the surface smoothness [28]. Then the Co film and the subsequently grown Pd, Pb, or Bi capping layers were deposited after the sample was cooled to room temperature. During film growth, the deposition rate and the thickness or coverage of the Pd, Pb, and Bi were monitored through medium-energy electron diffraction (MEED). The growth conditions of Pd, Pb, and Bi on Co/Ni/Cu were also investigated at room temperature using an Auger electron spectrum (AES), which employed a single-path cylindrical mirror analyzer (CMA). The in-plane atomic structure of the films was measured using low-energy electron diffraction (LEED) at 130 eV in room temperature. The magnetic hysteresis loops of the samples were measured *in situ* through magneto-optical Kerr effects (MOKE) in both longitudinal and polar geometries at room temperature. The influences of Pd, Pb, and Bi adsorption on the magnetic properties of the interfacial Co layer were examined by assessing the x-ray magnetic circular dichroism (XMCD) effects with sum-rule analysis [29] at the Co $L_{3,2}$ absorption edges in total electron yield mode; these measurements were performed at an end station of x-ray photoemission electron microscopy (PEEM) [30–32] at beamline BL05B2 of the National Synchrotron Radiation Research Center in Hsinchu, Taiwan. The measurements of x-ray absorption spectrum (XAS) and XMCD curves were performed under remanent conditions at room temperature, achieved by applying either positive or negative magnetic

fields along the in-plane (± 200 Oe) or out-of-plane directions (± 1000 Oe) before placing it in the PEEM sample holder. The XAS were normalized by the incident beam intensity as well as the edge jump of $L_{3,2}$.

III. RESULTS

A. Growth of Pd, Pb, Bi on 2-ML Co/15-ML Ni/Cu(001)

Figure 1 depicts the typical specular reflection MEED (0,0) beam intensity of various growth materials as a function of deposition time. Regarding Ni grown on Cu(001), Co on 15-ML Ni/Cu(001), and Pd on Co/Ni/Cu, the presence of regular oscillation indicates layer-by-layer growth conditions for these films. By contrast, the MEED curves of the Pb and Bi grown on Co/Ni/Cu exhibit merely one distinguishable peak at the initial stage of the growth. This result suggests that a flat surface of Pb or Bi grown on Co/Ni/Cu is present only at low coverage. The growth conditions of Pd, Pb, and Bi on Co/Ni/Cu were further examined using AES by applying CMA. According to AES theory [33,34], the contribution of the AES signal from the buried layer decays exponentially when the distance to the top surface of the covered layer is increased. Thus, the growth conditions of the deposited materials can be distinguished by examining the AES peak ratio between the deposited material and underlayer (i.e., $I_{\text{deposition}}/I_{\text{underlayer}}$), according to the coverage-dependent AES curves. Figures 2(a)–2(c) display the ratios of 0–4-ML Pd, Pb, and Bi/Co/Ni/Cu recorded from the Pd (318–330 eV),

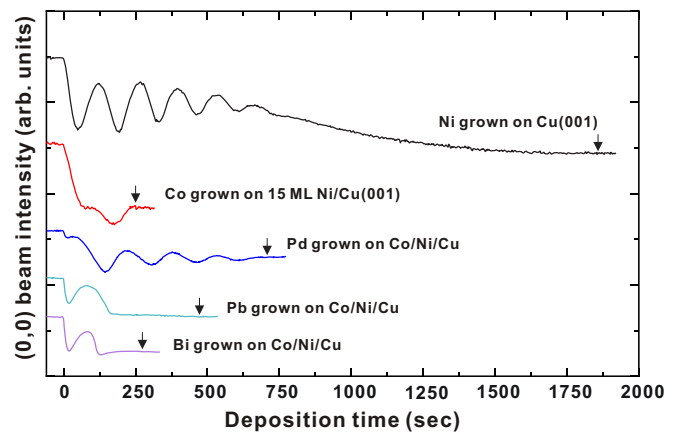


FIG. 1. Selected MEED (0,0) beam intensity curves as a function of deposition time for Ni grown on Cu(001); Co grown on 15-ML Ni/Cu(001); and Pd, Pb, and Bi grown on Co/Ni/Cu at 300 K. Film thickness or coverage was calibrated by the oscillations in the MEED curves. Arrows indicate the time taken for the shutter to be closed.

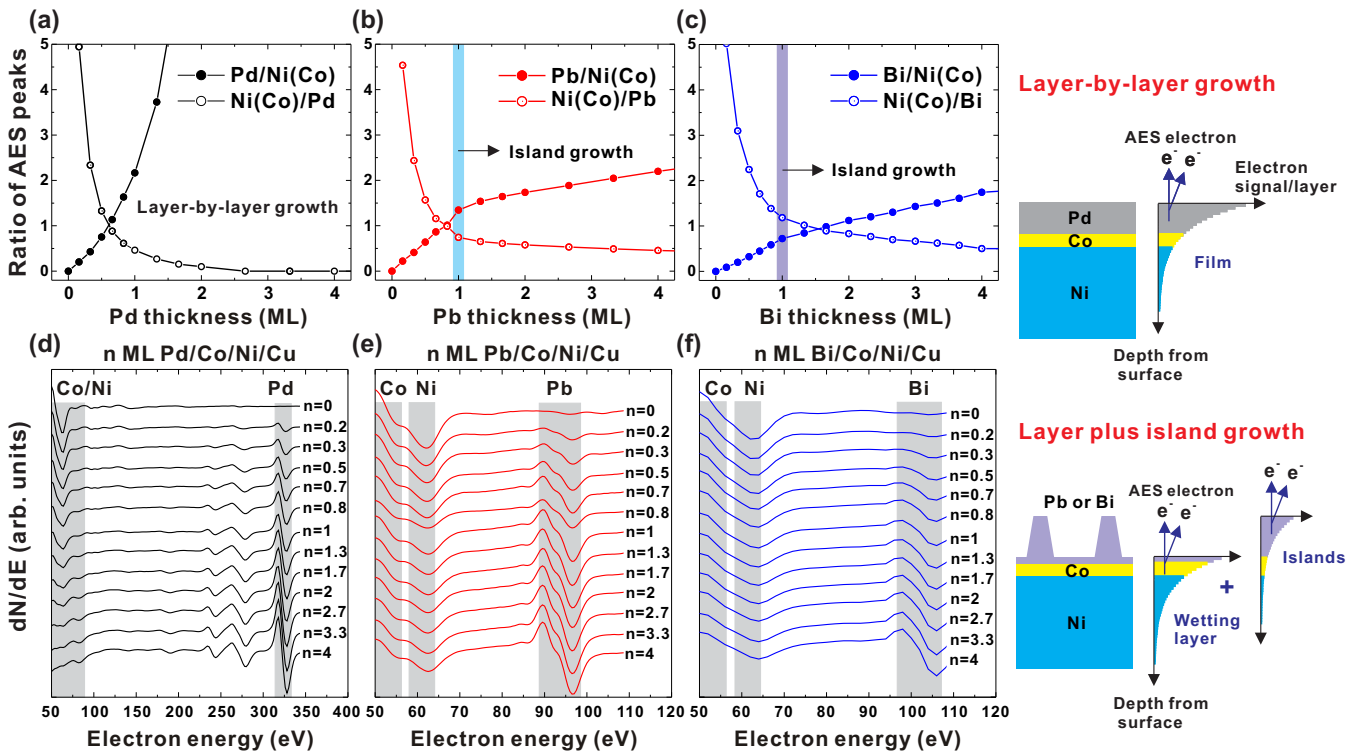


FIG. 2. (a)–(c) Summarized AES peak high ratios between grown materials (Pd, Pb, and Bi) and Co/Ni films as functions of Pd, Pb, and Bi coverage, according to AES curves displayed in (d)–(f), respectively. Schematic on the right displays the contribution of the film, wetting layer, and three-dimensional islands to AES signals under different growth modes.

Pb (88–100 eV), Bi (98–106 eV), and Co/Ni (50–64 eV) peaks displayed in the dN/dE AES curves of Figs. 2(d)–2(f) [35]. Considering Pd grown on Co/Ni/Cu [Fig. 2(a)], we observed significantly enhanced $I_{Pd}/I_{Co/Ni}$ when Pd coverage (t_{Pd}) increases. This behavior is typically associated with the layer-by-layer (van der Merve) growth mode [33,34] because of the significantly increased average distance between the Pd film surface and the Co underlayer; this result is also consistent with an observation of regular oscillation in the MEED curve (Fig. 1). Regarding the initial stage of the growth of Pb(Bi) on Co/Ni/Cu [Figs. 2(b) and 2(c)], the $I_{Pb}/I_{Co/Ni}$ ($I_{Bi}/I_{Co/Ni}$) increases linearly with Pb(Bi) coverage t_{Pd} (t_{Bi}). Upon t_{Pd} (t_{Bi}) exceeding approximately 1 ML, the slope of $I_{Pb}/I_{Co/Ni}$ ($I_{Bi}/I_{Co/Ni}$) suddenly decreases. This characteristic behavior is typically linked to the layer-plus-island (Stranski-Krastanov) growth mode [33,34], where a 1-ML wetting layer forms at the interface before the growth of the three-dimensional islands. Thus, the presence of a single peak in the Pb(Bi) MEED curves (Fig. 1) can be attributed to a formation of a 1-ML wetting layer.

The different growth modes between the Pd and Pb(Bi) on Co/Ni/Cu could be understood through the concept of interplay among the surface free, cohesive, and strain energies. The surface free energy is commonly defined as the work required to construct the unit area of a particular surface or interface [36]. As displayed in Table II, the surface free energy of the Pd, Pb, and Bi layers are lower than that of the Co layer. Therefore, in the initial stage of growth, due to the lower strain energy, the deposited atoms prefer to form a wetting layer on the Co surface, which can reduce the exposed area of the Co

layer and the total surface/interface free energy of the system. For the subsequently deposited atoms, however, the growth conditions depend on the competition between the strain energy and cohesive energy within the grown materials [34]. For the grown film with large strain energy, the atoms prefer to reduce the strain energy by forming either strain-relaxed films or three-dimensional islands. In the present work, Pd atoms grown in a $p(1 \times 1)$ structure of the Co/Ni/Cu are under a compressive strain (-7.7%). Because of relatively high cohesive energy (Table II) [37], moving the Pd atoms across different surface steps to form relaxed three-dimensional islands entails a substantial energy cost. Thus, the added Pd atoms tended to maintain their filmlike shape. By contrast, the Pb(Bi) layers grown in $c(2 \times 2)$ structure of the Co/Ni/Cu are subject to a tensile strain of 3.3% (6.1%). However, due to the relatively low cohesive energy (Table II), the added Pb(Bi) atoms are more prone to growing into relaxed three-dimensional islands to reduce the large strain energy, although limited surface free energy is gained due to the formation of islands on the wetting layer.

B. Surface crystalline structure of Pd, Pb, Bi on Co/Ni/Cu

The in-plane surface structures of Pd, Pb, and Bi/Co/Ni/Cu were investigated using LEED at 130 eV. Regarding 1-ML Pd/Co/Ni/Cu [Fig. 3(c)], characteristic $p(1 \times 1)$ spots locate at the same positions as those of the Cu(001) [Fig. 3(a)] and Co/Ni/Cu [Fig. 3(b)]. This indicates an epitaxial growth condition for the grown 1-ML Pd film; the in-plane lattice constant ($a_{||}$) of 1-ML Pd is determined

TABLE II. Surface free energy of Pd, Pb, Bi, Co, Ni, and Cu at the {100} surfaces [25,26], and the cohesive energy (energy required to separate the atoms) in units of eV/atom [37].

Elements	Pd	Pb	Bi	Co	Ni	Cu
Surface free energy [25,26]	0.95	0.46	0.30	0.98	0.94	0.74
Cohesive energy [37]	3.89	2.03	2.18	4.39	4.44	3.49

to be equal to 3.61 \AA [lattice constant of Cu(001)]. When t_{Pd} reaches 2 and 3 ML [Figs. 3(d) and 3(e)], the $p(1 \times 1)$ spots disappear. This behavior indicates a formation of structurally disordered Pd layers, probably caused by a large lattice mismatch between the Pd and Co/Ni/Cu (Table I). Regarding Pb grown on Co/Ni/Cu [Fig. 3(f)], not only sharp $p(1 \times 1)$ but also $c(2 \times 2)$ LEED spots are present at $t_{\text{Pb}} = 1 \text{ ML}$. This finding suggests the formation of an ordered Pb wetting layer with atoms occupying the $c(2 \times 2)$ sites of the Co/Ni/Cu; this is similar to the behaviors of Pb grown on Ni(001) or Cu(001) [38,39]. Thus, the atomic density of 1-ML Pb (or 1-ML Bi introduced in the latter) defined in the present work is half of the Cu(100) [Cu(001): $1.53 \times 10^{15} \text{ atoms/cm}^2$] [26]. However, the lattice structure of the Pb layer evolves with t_{Pb} . When t_{Pb} is larger than 1 ML [Figs. 3(g) and 3(h)], those $c(2 \times 2)$ spots split into four arclike features. Such a superstructure becomes clear when t_{Pb} is increased to approximately 2 ML, but then gradually disappears when t_{Pb} is increased to 3 ML. Meanwhile, the $p(1 \times 1)$ spots remain clear. Considering

Bi grown on Co/Ni/Cu, sharp $p(1 \times 1)$ and $c(2 \times 2)$ LEED spots are also present when t_{Bi} reaches 1 ML [Fig. 3(i)]; this is similar to the behavior of Bi grown on Cu(001) [40]. However, the $c(2 \times 2)$ spots soon became blurred when t_{Bi} is higher than 1 ML [Figs. 3(j) and 3(k)].

The detailed atomic model of the Pb(Bi) wetting layer affected by the addition of Pb(Bi) atom adsorption is discussed in the following. According to the current LEED results [Fig. 3(f)], $c(2 \times 2)$ spots are present in Pb/Co/Ni/Cu when $t_{\text{Pb}} = 1 \text{ ML}$. When $t_{\text{Pb}} > 1 \text{ ML}$, four arclike superstructures, moved from $c(2 \times 2)$ sites toward four symmetric 45° directions, begin to set in [Fig. 3(g)]. A formation of such superstructures around the $c(2 \times 2)$ sites is attributable to a change in the atomic structure of the Pb wetting layer upon adsorption of the added atoms. Figure 4(a) presents the schematic atomic models of the Pb wetting layer [$c(2 \times 2)$ stacking], Co film [$p(1 \times 1)$ stacking], and the corresponding LEED patterns. According to a comparison of the reciprocal distances of the four arclike superstructures and the $c(2 \times 2)$

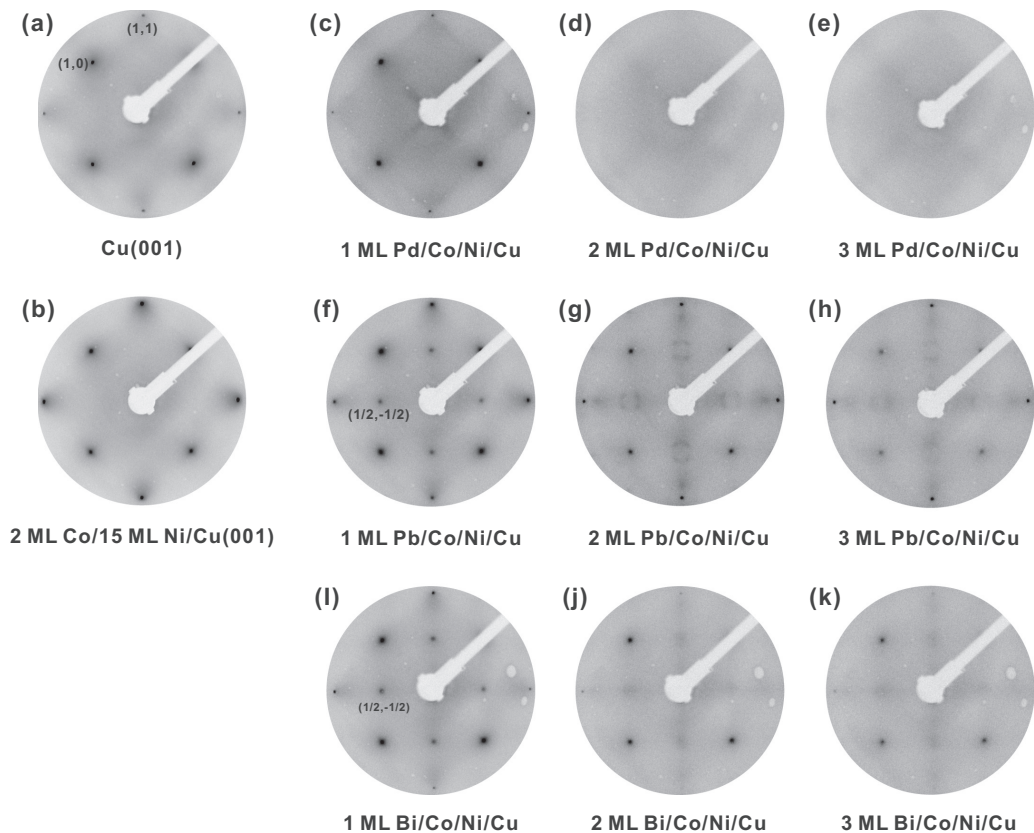


FIG. 3. LEED patterns of (a) Cu(001), (b) Co/Ni/Cu, (c)–(e) 1–3-ML Pd/Co/Ni/Cu, (f)–(h) 1–3-ML Pb/Co/Ni/Cu, and (i)–(k) 1–3-ML Bi/Co/Ni/Cu, measured at 130 eV and 300 K. The atomic densities of 1-ML Pd and 1-ML Pb(Bi) are the same and half the surface atoms of Cu(001), respectively.

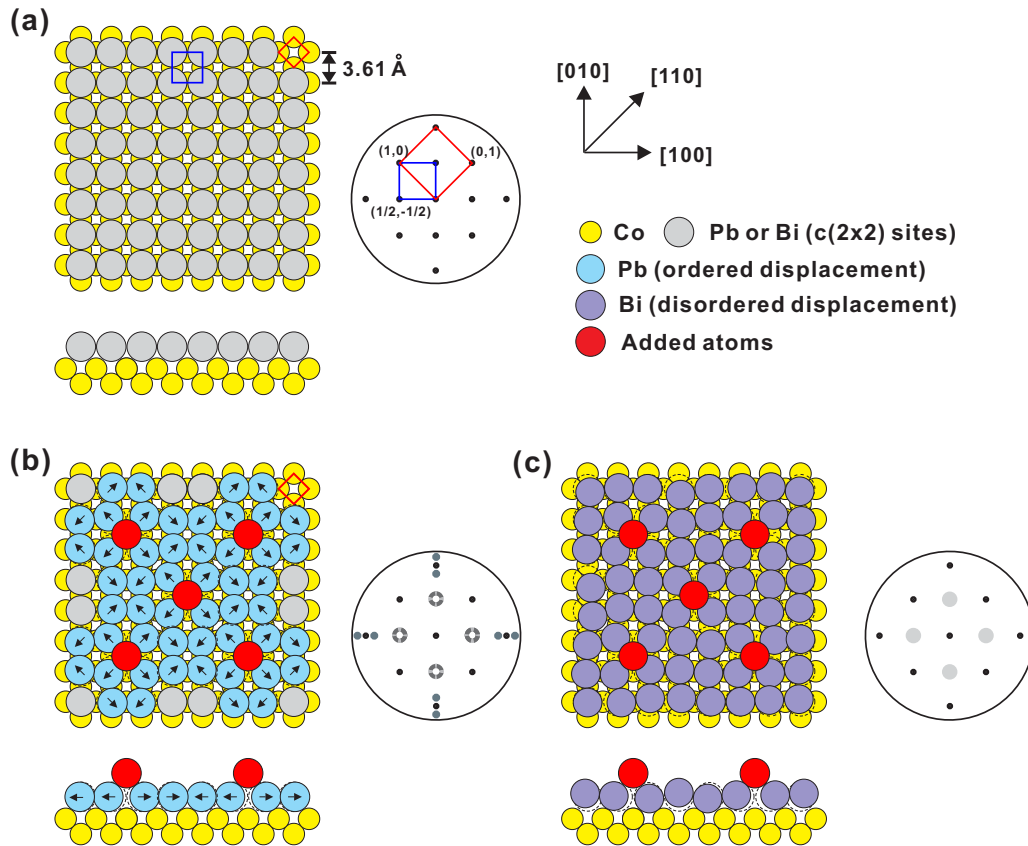


FIG. 4. Schematic of atomic models (top and side views) of 1-ML Pb(Bi) grown on $c(2 \times 2)$ sites of Co/Ni/Cu. The unit cells of the Co (red) and Pb(Bi) (blue) in real and reciprocal spaces are displayed in the diagrams. (b) and (c) Schematics of atomic models (top and side view) for 1-ML Pb/Co/Ni/Cu and 1-ML Bi/Co/Ni/Cu under the adsorption of Pb- and Bi-added atoms, respectively. In (a)–(c), the corresponding LEED patterns are displayed on the right. In (b) and (c), the dashed circles in the atomic models indicate the positions of $c(2 \times 2)$ sites. In (b), the arrows indicate an ordered displacement of Pb atoms in the four $\{110\}$ directions. In (c), the displacement of Bi atoms in the wetting layer are disordered.

spots [Fig. 3(g)], an ordered displacement of approximately 0.5 \AA toward $\{110\}$ directions in the wetting layer is estimated. Such a displacement could be attributed to a strain relief of the Pb wetting layer triggered by repulsive force from the added Pb atoms located at the interstitial sites of the wetting layer, as illustrated in the schematic atomic model of Fig. 4(b), and this finding is supported by a prior study of Pb(Bi) grown on Cu(001) [41] which shows that Pb or Bi atoms prefer to stack or displace along the $\{110\}$ directions. However, although similar $c(2 \times 2)$ LEED spots are also present in 1-ML Bi/Co/Ni/Cu [Fig. 3(i)], blurry $c(2 \times 2)$ spots are present when $t_{\text{Bi}} > 1 \text{ ML}$ [Figs. 3(j) and 3(k)]. Meanwhile, because the $p(1 \times 1)$ LEED spots remain sharp, an observation of blurry $c(2 \times 2)$ spots suggests a disordered structure of the Bi wetting layer, as displayed in the schematic in Fig. 4(c). Thus, in contrast to an ordered structure of the Pb wetting layer under the strain relief, Bi wetting layer shows a disordered structure. The different evolutions of the structure of the wetting layer between the Pb and Bi/Co/Ni/Cu under the layer-plus-island growth mode could be understood through a comparison of their strain level and cohesive energy. Although the cohesive energy between Pb and Bi are similar (Table II), the strain level for the Bi wetting layer grown in the $c(2 \times 2)$ structure of Co/Ni/Cu(001) is twice that of Pb (Table I). With

the accumulation of larger tensile strain, the direction of strain relaxation of the atoms in Bi wetting layer under the layer-plus-islands growth mode could be more random than that in Pb wetting layer; this could therefore result in a relatively disordered structure of the Bi wetting layer in Bi/Co/Ni/Cu when $t_{\text{Bi}} > 1 \text{ ML}$.

C. Magnetic properties of Pd, Pb, Bi/Co/Ni/Cu

Figure 5(a) illustrates the magnetic hysteresis loops of 0–4-ML Pd grown on in-plane magnetic Co/Ni/Cu, which indicates that PMA can be triggered when t_{Pd} is greater than 0.7 ML (1-ML Pd: $1.53 \times 10^{15} \text{ atoms/cm}^2$). According to Fig. 5(d), the perpendicular H_c value maintains a similar level of 50–40 Oe when t_{Pd} varies between 1 and 4 ML; this indicates that once the 1-ML Pd film is covered, the strength of PMA in Pd/Co/Ni/Cu varies slowly with variations in t_{Pd} . Regarding Pb/Co/Ni/Cu [Fig. 5(b)], PMA can be triggered and then enhanced when $t_{\text{Pb}} > 0.6 \text{ ML}$ [1-ML Pb(Bi): $0.76 \times 10^{15} \text{ atoms/cm}^2$]. However, after reaching a maximum value ($\approx 160 \text{ Oe}$) at a t_{Pb} of approximately 2 ML [Fig. 5(e)], increasing t_{Pb} tends to reduce the perpendicular H_c . The non-trivial behavior of induced PMA with a variation of capping layer in thickness is also present in Bi/Co/Ni/Cu [Figs. 5(c)

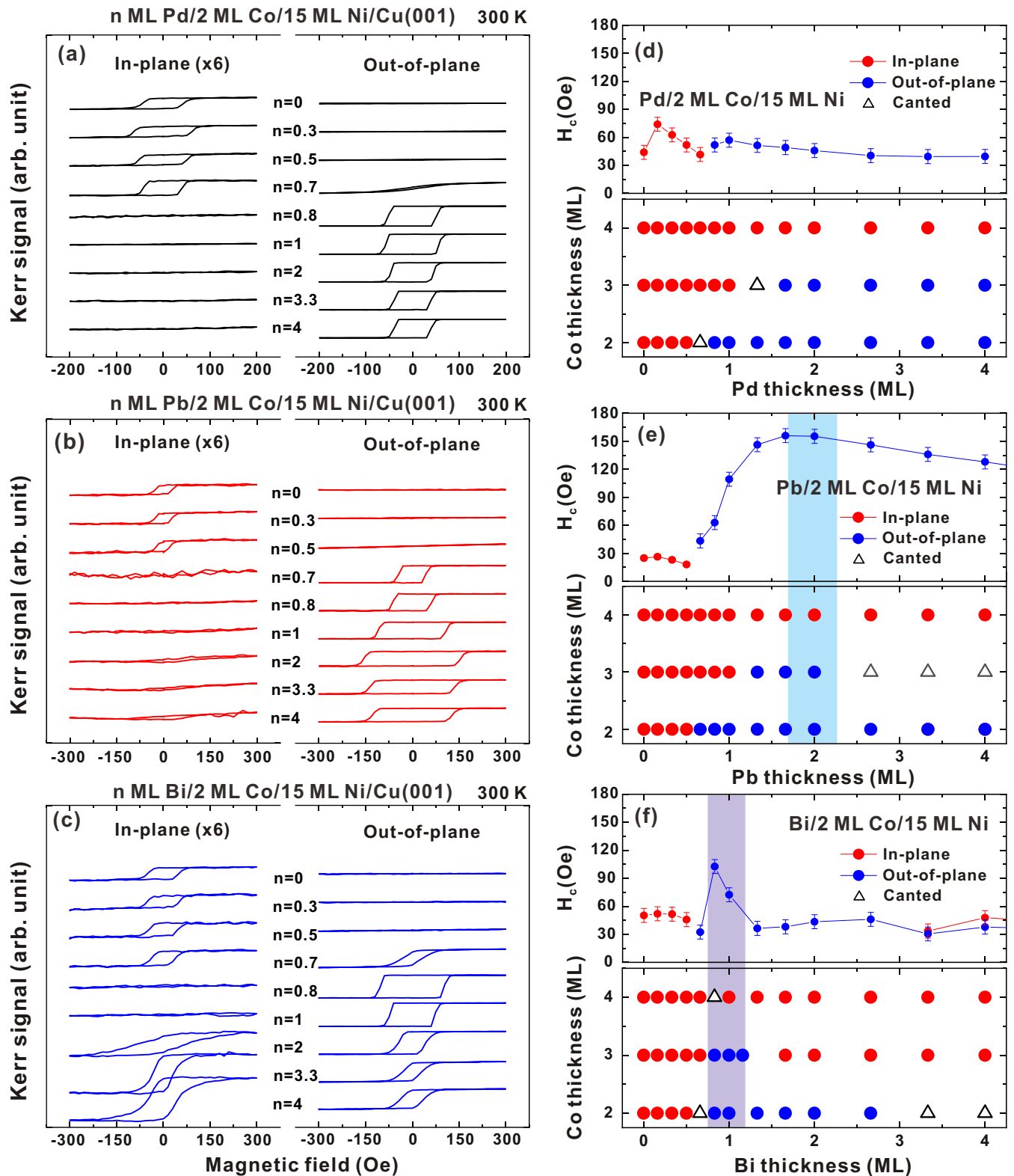


FIG. 5. Magnetic hysteresis loops of (a) 0–4-ML Pd/Co/Ni/Cu, (b) 0–4-ML Pb/Co/Ni/Cu, and (c) 0–4-ML Bi/Co/Ni/Cu measured according to the longitudinal and polar MOKE at 300 K. The summarized H_c values, in accordance with (a), (b), and (c), are displayed in the upper sections of (d), (e), and (f), respectively. The lower sections of (d), (e), and (f) display the magnetic easy axis phase diagram of 0–4-ML Pd/2–4-ML Co/15-ML Ni/Cu(001), 0–4-ML Pb/2–4-ML Co/15-ML Ni/Cu(001), and 0–4-ML Bi/2–4-ML Co/15-ML Ni/Cu(001), respectively. In (e) and (f), the color shadows denote the estimated critical ranges of t_{pb} and t_{Bi} , which cause the maximum intensity of PMA on the Pb(Bi)/Co/Ni films.

TABLE III. Orbit-to-spin ratio ($m_{\text{orbit}}/m_{\text{spin}}$) of Co moments in various Pd, Pb, and Bi/Co/Ni/Cu. The symbol \parallel (\perp) denotes the in-plane (perpendicular) magnetic easy directions of the films.

Systems	$m_{\text{orbit}}/m_{\text{spin}}$ ($n = 0$)	$m_{\text{orbit}}/m_{\text{spin}}$ ($n = 1$)	$m_{\text{orbit}}/m_{\text{spin}}$ ($n = 2$)
n -ML Pd/Co/Ni	0.11 ± 0.02 (\parallel)	0.13 ± 0.02 (\perp)	0.13 ± 0.02 (\perp)
n -ML Pb/Co/Ni		0.22 ± 0.02 (\perp)	0.27 ± 0.02 (\perp)
n -ML Bi/Co/Ni		0.22 ± 0.02 (\perp)	0.20 ± 0.02 (\perp)

and 5(f)]; the perpendicular H_c is induced when $t_{\text{Bi}} > 0.7$ ML but then is significantly decreased after achieving a maximum value (≈ 100 Oe) at a t_{Bi} of approximately 1 ML. The lower sections of Figs. 5(d)–5(f) further display the magnetic easy axis phase diagrams of various 0–4-ML Pd, Pb, and Bi/2–4 ML Co/15-ML Ni/Cu(001). Notably, the thickness ranges of the capping metals that trigger PMA are reduced when the thickness of the Co layer is increased. This behavior can be attributed to a significantly enhanced in-plane shape anisotropy and in-plane MCA in a thicker Co film [42]. Thus, by tuning the level of in-plane magnetic anisotropy of the Co/15-ML Ni/Cu(001), we could obtain the critical ranges of t_{Pd} , t_{Pb} , and t_{Bi} that trigger maximum PMA. Regarding Pd/Co/15-ML Ni/Cu(001), increasing Co thickness from 2 to 3 ML results in only a slight delay in triggering PMA after the t_{Pd} threshold is crossed; the PMA is not decreased further when t_{Pd} is increased. For Pb(Bi)/Co/15-ML Ni/Cu(001), by contrast, a maximum PMA is triggered when $t_{\text{Pb}}(t_{\text{Bi}})$ approaches approximately 2(1) ML; these critical values are consistent with the results estimated from the maximum value of perpendicular H_c on these systems [displayed in the upper sections of Figs. 5(e) and 5(f)]. According to current MOKE results, the magnetic anisotropy energy contributed by the Pd, Pb, and Bi atoms at the interface can also be estimated by applying Néel type phenomenological model [43]. According to the analysis detailed in the Supplemental Material [44], the perpendicular anisotropy energy contributed by Pd, Pb, and Bi wetting layers per atom (unit area) were estimated to be 285.4, 652.0, and 570.8 $\mu\text{eV}/\text{atom}$ (0.70, 0.80, and 0.70 mJ/m^2), respectively. These values indicate a large perpendicular interface anisotropy energy engendered by 6*p*-HMs, when only half the atom density in Pb and Bi wetting layers (compared with Pd) are considered.

To clarify the origin of the induced PMA in Pd, Pb, Bi/Co/Ni/Cu, Fig. 6 displays the XAS and XMCD curves measured at the Co $L_{3,2}$ edges. The p and q values given by the integration of the XMCD curve in the L_3 and $L_3 + L_2$ regions, respectively, indicate the sum of magnetic asymmetry in both regions. According to XMCD sum rules [29], extracting the ratio of orbit to spin moments ($m_{\text{orbit}}/m_{\text{spin}}$) of a magnetic sample requires only information of the p and q values from XMCD curves. In addition, the effects of the thermal perturbation on the remanent magnetization can be offset by the $m_{\text{orbit}}/m_{\text{spin}}$ normalization. Thus, instead of the m_{orbit} and m_{spin} values, we extract $m_{\text{orbit}}/m_{\text{spin}}$ ratio of a series of Pd, Pb, Bi/Co/Ni/Cu samples for a comparison. Assume a negligible magnetic dipole operator term in the spin sum rule [45,46], which is small for 3*d* metals [47]. Next, p and q values can be used to calculate $m_{\text{orbit}}/m_{\text{spin}}$ ratio according to the formula of $m_{\text{orbit}}/m_{\text{spin}} = 2q/(9p - 6q)$ [29], thereby obtaining information on MCA [21,48–50]. Table III summarizes the

results of the $m_{\text{orbit}}/m_{\text{spin}}$ ratio of the Co moments in various samples. Compared with in-plane magnetic Co/Ni/Cu, an increase in the $m_{\text{orbit}}/m_{\text{spin}}$ ratio is present in perpendicularly magnetic Pd, Pb, and Bi/Co/Ni/Cu. This confirms the notion of an increase in the perpendicular MCA (spin-orbit coupling) of the interfacial Co moments to be the origin of the established PMA in these systems; this could be triggered by orbital hybridization with the capping layers at the interface [23,51–53]. Moreover, as indicated in Table III, the $m_{\text{orbit}}/m_{\text{spin}}$ ratio of the Co moments in Pb(Bi)/Co/Ni/Cu is much larger than that in Pd/Co/Ni/Cu. According to the literature [21,23], the MCA energy driven by spin-orbit coupling is proportional to the square of the spin-orbit coupling constant. Thus, the 6*p*-Pb and Bi atoms at the interface could generate a higher strength of perpendicular MCA relative to the 4*d*-Pd atoms, because the spin-orbit coupling constant of 6*p*-HMs is larger than that of 4*d* metals [21]. In addition, by comparing the $m_{\text{orbit}}/m_{\text{spin}}$ ratio of the Co moments in either Pb/Co/Ni/Cu or Bi/Co/Ni/Cu, relatively higher values are present for t_{Pb} (2 ML) and t_{Bi} (1 ML). This result indicates that the perpendicular MCA of the interfacial Co layer engendered by orbital hybridization from Pb(Bi) atoms is also sensitive to a variation of $t_{\text{Pb}}(t_{\text{Bi}})$, which accords with observations of nontrivial $t_{\text{Pb}}(t_{\text{Bi}})$ -dependent behavior of induced PMA in these samples [Figs. 5(e) and 5(f)].

IV. DISCUSSION

A. PMA induced by 6*p*-Pb, Bi atomic layers: Crucial effects of interface structural order

In the current work, compared with 4*d*-Pd/Co/Ni/Cu, 6*p*-Pb(Bi)/Co/Ni/Cu exhibits a strongly enhanced PMA and out-of-plane $m_{\text{orbit}}/m_{\text{spin}}$ ratio of the Co moment (Table III); this verifies a giant interfacial MCA and spin-orbit coupling triggered by 6*p*-HMs through a 6*p*-3*d* orbital hybridization at interface, as theoretically proposed by Peng *et al.* [23]. However, the PMA-induction behaviors of the Pb/Co/Ni/Cu and Bi/Co/Ni/Cu in the present work are quite different, especially for $t_{\text{Pb}}(t_{\text{Bi}}) > 1$ ML (Fig. 5). We speculate that this is related to the differences found in the surface structure of Pb(Bi) (LEED patterns in Fig. 3) and the orbital hybridization of Pb(Bi)-Co interface ($m_{\text{orbit}}/m_{\text{spin}}$ value of the Co layer extracted from Co $L_{3,2}$ XMCD curves in Fig. 6). Regarding 1-ML Pb/Co/Ni/Cu and 1-ML Bi/Co/Ni/Cu showing ordered $c(2 \times 2)$ surface structure [Figs. 3(f) and 3(i)], the extracted $m_{\text{orbit}}/m_{\text{spin}}$ values of the Co layers are in a similar level (≈ 0.22) [Figs. 6(c) and 6(e)]. This indicates a similar orbital hybridization effects at the Pb(Bi)-Co interfaces in these two systems, which can be understood from their similar atomic orbitals in valence shells and similar degree of interface

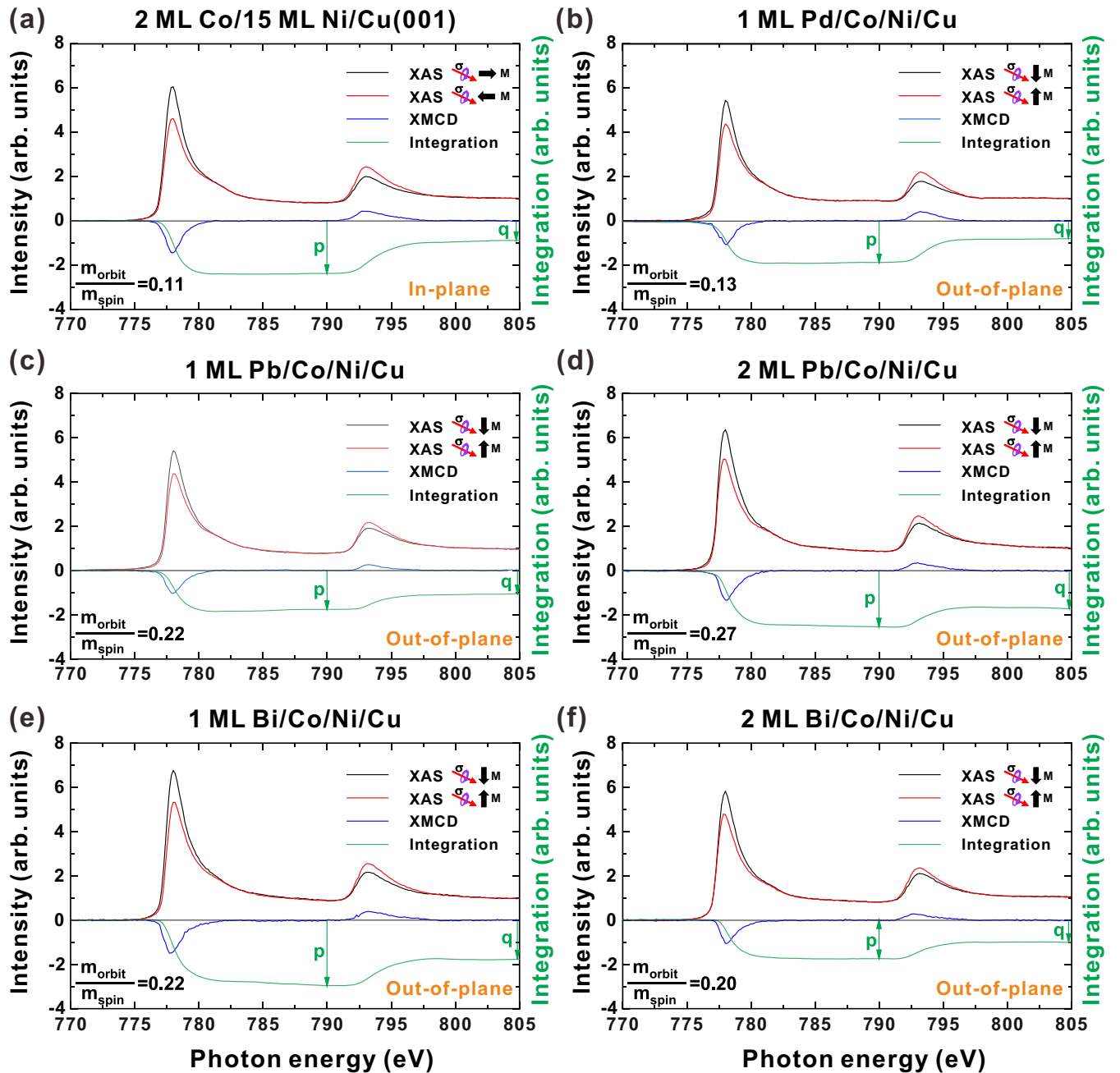


FIG. 6. XAS and XMCD curves of (a) Co/Ni/Cu, (b) 1-ML Pd/Co/Ni/Cu, (c) and (d) 1- and 2-ML Pb/Co/Ni/Cu. (e) and (f) 1- and 2-ML Bi/Co/Ni/Cu measured at the Co $L_{3,2}$ edges in remanent states. The angle of incidence in circular-polarized x rays was 25° with respect to the in-plane [010] crystallographic direction of Cu(001). The orbit-to-spin ratios ($m_{\text{orbit}}/m_{\text{spin}}$) of Co moments were extracted from the integration of the XMCD curves according to the XMCD sum-rule data [29].

structural order. By contrast, the extracted $m_{\text{orbit}}/m_{\text{spin}}$ value of the Co layer in 2-ML Bi/Co/Ni/Cu (≈ 0.20) is relatively lower than in 2-ML Pb/Co/Ni/Cu (≈ 0.27) [Figs. 6(d) and 6(f)]. This suggests that the orbital hybridization effects occurred at the 2-ML Bi-Co interface could be relatively weaker than at the 2-ML Pb-Co interface, which could be associated with a relatively disordered surface structure of the 2-ML Bi compared to 2-ML Pb according to the LEED results [Figs. 3(g) and 3(j)]. Indeed, according to prior reports [51–53], the PMA of a FM film promoted by a thin capping layer is typically triggered by an enhanced orbital moment

at the interface, which in turn is due to the band narrowing caused by the loss of atomic neighbors. However, the narrowing of the density of state at the interface would be reduced when the degree of disorder in the capping layer is increased. In the present work we speculate that such an effect could result in a reduction of the orbital hybridization effects and the induced PMA in 2-ML Bi/Co/Ni/Cu, when compare to 2-ML Pb/Co/Ni/Cu. In summary, current results show that 1-ML Pb/Co/Ni/Cu and 1-ML Bi/Co/Ni/Cu exhibit similar PMA-induction behaviors; this could be attributed to the similar $6p$ atomic orbital of Pb(Bi) in valence shells and

similar degree of structural order at the Pb(Bi)-Co interfaces. However, the magnetic behaviors of Pb(Bi)/Co/Ni/Cu when $t_{\text{Pb(Bi)}} > 1$ ML should include contributions associated with the atomic ordering at the Pb(Bi)-Co interfaces; this argument can also be supported by a finding of similar evolution between the PMA and ordering of the surface structure in wedge-shaped 0–3-ML Pb(Bi)/Co/Ni/Cu samples detailed in the Supplemental Material [44].

According to the aforementioned discussion, the current study can further uncover the crucial effects of interface structural order (or disorder) of the $6p$ -HM wetting layers on the induced PMA as well as the spin-orbit coupling. In Pb/Co/Ni/Cu, the Pb wetting layer with an ordered atomic structure could ensure a high orbital hybridization between the $6p$ -Pb and $3d$ -Co orbitals at the interface. In addition, the added atoms at the ordered interstitial sites could also contribute to the Pb-Co interface orbital hybridization and thus could continually strengthen the PMA and spin-orbit coupling in Pb/Co/Ni/Cu until t_{Pb} is approximately 2 ML, for which the degree of disorder in the wetting layer starts to increase [44]. By contrast, the disordered structure of the Bi wetting layer induced by the added Bi atoms and greater strain may have hindered the orbital hybridization between the $6p$ -Bi and $3d$ -Co orbitals at the interface; therefore, this could have limited the promotion of PMA and spin-orbit coupling in Bi/Co/Ni/Cu when t_{Bi} is approximately 1 ML. Regarding the reference Pd/Co/Ni/Cu, because the atomic density of the Pd interfacial layer is twice of the Pb(Bi) wetting layers, the influence of orbital hybridization of Pd added atoms on Co layer through close-packed Pd interfacial layer could be relatively minor. The strength of PMA induced in Pd/Co/Ni/Cu films could therefore be insensitive to an increase in t_{Pd} [Figs. 5(a) and 5(d)]. Thus, current work clearly demonstrated that the PMA as well as the spin-orbit coupling engendered in HM-

FM systems through orbital hybridization at the interface are not only determined by the level of atomic orbital of the capping metals but are also highly sensitive to the ordering degree of the interfacial wetting layer. We expect our study findings can inspire more experimental or theoretical work to promote the key spin-orbit coupling effects of HM in HM-FM heterosystems, which will be indispensable to the application of HM in magnetic devices.

V. CONCLUSION

We comprehensively investigated the correlation between the interface structure order, orbital hybridization, and induced PMA (spin-orbit coupling) in a series of $6p$ -Pb(Bi) and $4d$ -Pd (reference) atomic layers grown on the in-plane magnetic Co/Ni/Cu. Our results demonstrate that the PMA engendered by the $6p$ -HMs through interface orbital hybridization are highly sensitive to the order degree of the interfacial wetting layers which is determined by the interplay of the surface free, cohesive, and strain energies within the grown materials. The $6p$ -HM atoms added on the wetting layer can enhance the PMA of the adjacent FM film only when the wetting layer maintains an ordered structure. The findings of this study unveil the critical interface effects of $6p$ -HMs on the FM layer and offer important clues for the promotion and development of low-power spintronic devices or even quantum materials that require high spin-orbit interaction engendered by HMs through the interface.

ACKNOWLEDGMENT

This work was partly supported by the Ministry of Science and Technology, Taiwan (Grant No. MOST 110-2112-M-018-007).

-
- [1] C. Chappert, A. Fert, and F. N. Van Dau, *Nat. Mater.* **6**, 813 (2007).
- [2] S. Ikeda, K. Miura, H. Yamamoto, K. Mizunuma, H. D. Gan, M. Endo, S. Kanai, J. Hayakawa, F. Matsukura, and H. Ohno, *Nat. Mater.* **9**, 721 (2010).
- [3] W.-G. Wang, M. Li, S. Hageman, and C. L. Chien, *Nat. Mater.* **11**, 64 (2011).
- [4] G. Yu, P. Upadhyaya, Y. Fan, J. G. Alzate, W. Jiang, K. L. Wong, S. Takei, S. A. Bender, L. Chang, Y. Jiang, M. Lang, J. Tang, Y. Wang, Y. Tserkovnyak, P. K. Amiri, and K. L. Wang, *Nat. Nanotechnol.* **9**, 548 (2014).
- [5] F. A. Cuellar, Y. H. Liu, J. Salafranca, N. Nemes, E. Iborra, G. Sanchez-Santolino, M. Varela, M. G. Hernandez, J. W. Freeland, M. Zhernenkov, M. R. Fitzsimmons, S. Okamoto, S. J. Pennycook, M. Bibes, A. Barthélemy, S. G. E. Te Velthuis, Z. Sefrioui, C. Leon, and J. Santamaria, *Nat. Commun.* **5**, 4215 (2014).
- [6] D. C. Worledge, G. Hu, D. W. Abraham, J. Z. Sun, P. L. Trouilloud, J. Nowak, S. Brown, M. C. Gaidis, E. J. Ó. Sullivan, and R. P. Robertazzi, *Appl. Phys. Lett.* **98**, 022501 (2011).
- [7] I. M. Miron, K. Garello, G. Gaudin, P.-J. Zermatten, M. V. Costache, S. Auffret, S. Bandiera, B. Rodmacq, A. Schuhl, and P. Gambardella, *Nature (London)* **476**, 189 (2011).
- [8] L. Liu, C.-F. Pai, Y. Li, H. W. Tseng, D. C. Ralph, and R. A. Buhrman, *Science* **336**, 555 (2012).
- [9] M. Cubukcu, O. Boulle, M. Drouard, K. Garello, C. O. Avci, I. M. Miron, J. Langer, B. Ocker, P. Gambardella, and G. Gaudin, *Appl. Phys. Lett.* **104**, 042406 (2014).
- [10] K. Garello, C. O. Avci, I. M. Miron, M. Baumgartner, A. Ghosh, S. Auffret, O. Boulle, G. Gaudin, and P. Gambardella, *Appl. Phys. Lett.* **105**, 212402 (2014).
- [11] N. Perez, E. Martinez, L. Torres, S.-H. Woo, S. Emori, and G. S. D. Beach, *Appl. Phys. Lett.* **104**, 092403 (2014).
- [12] C. Zhang, S. Fukami, H. Sato, F. Matsukura, and H. Ohno, *Appl. Phys. Lett.* **107**, 012401 (2015).
- [13] A. Ghosh, K. Garello, C. O. Avci, M. Gabureac, and P. Gambardella, *Phys. Rev. Appl.* **7**, 014004 (2017).
- [14] C.-Z. Chang, J. Zhang, X. Feng, J. Shen, Z. Zhang, M. Guo, K. Li, Y. Ou, P. Wei, L.-L. Wang, Z.-Q. Ji, Y. Feng, S. Ji, X. Chen, J. Jia, X. Dai, Z. Fang, S.-C. Zhang, K. He, Y. Wang *et al.*, *Science* **340**, 167 (2013).
- [15] Y. Xu, B. Yan, H.-J. Zhang, J. Wang, G. Xu, P. Tang, W. Duan, and S.-C. Zhang, *Phys. Rev. Lett.* **111**, 136804 (2013).

- [16] A. Molle, J. Goldberger, M. Houssa, Y. Xu, S.-C. Zhang, and D. Akinwande, *Nat. Mater.* **16**, 163 (2017).
- [17] F.-F. Zhu, W.-J. Chen, Y. Xu, C.-L. Gao, D.-D. Guan, C.-H. Liu, D. Qian, S.-C. Zhang, and J.-F. Jia, *Nat. Mater.* **14**, 1020 (2015).
- [18] Z. Liu, C.-X. Liu, Y.-S. Wu, W.-H. Duan, F. Liu, and J. Wu, *Phys. Rev. Lett.* **107**, 136805 (2011).
- [19] Z. Fei, T. Palomaki, S. Wu, W. Zhao, X. Cai, B. Sun, P. Nguyen, J. Finney, X. Xu, and D. H. Cobden, *Nat. Phys.* **13**, 677 (2017).
- [20] J. Deng, B. Xia, X. Ma, H. Chen, H. Shan, X. Zhai, B. Li, A. Zhao, Y. Xu, W. Duan, S.-C. Zhang, B. Wang, and J. G. Hou, *Nat. Mater.* **17**, 1081 (2018).
- [21] J. Stöhr and H. C. Siegmann, *Magnetism: From Fundamentals to Nanoscale Dynamics* (Springer, New York, 2006).
- [22] X. Ma and J. Hu, *Appl. Mater. Interfaces* **10**, 13181 (2018).
- [23] S. Peng, W. Zhao, J. Qiao, L. Su, J. Zhou, H. Yang, Q. Zhang, Y. Zhang, C. Grezes, P. K. Amiri, and K. L. Wang, *Appl. Phys. Lett.* **110**, 072403 (2017).
- [24] Y. Zhang, X. Yang, P. Li, J. Ouyang, and M. Wu, *IEEE Magn. Lett.* **10**, 4503504 (2019).
- [25] L. Vitos, A. V. Ruban, H. L. Skriver, and J. Kollar, *Surf. Sci.* **411**, 186 (1998).
- [26] D. P. Woodruff and E. Vlieg, *Surface Alloys and Alloy Surfaces*, edited by D. P. Woodruff (Elsevier, Amsterdam, 2002).
- [27] B.-Y. Wang, P.-H. Lin, M.-S. Tsai, C.-W. Shih, M.-J. Lee, C.-W. Huang, N.-Y. Jih, P.-Y. Cheng, and D.-H. Wei, *Phys. Rev. B* **92**, 214435 (2015).
- [28] J. Shen, J. Giergiel, and J. Kirschner, *Phys. Rev. B* **52**, 8454 (1995).
- [29] C. T. Chen, Y. U. Idzerda, H. J. Lin, N. V. Smith, G. Meigs, E. Chaban, G. H. Ho, E. Pellegrin, and F. Sette, *Phys. Rev. Lett.* **75**, 152 (1995).
- [30] J. Stöhr, Y. Wu, B. D. Hermsmeier, M. G. Samant, G. R. Harp, S. Koranda, D. Dunham, and B. P. Tonner, *Science* **259**, 658 (1993).
- [31] C. M. Schneider and G. Schönhense, *Rep. Prog. Phys.* **65**, R1785 (2002).
- [32] D.-H. Wei, Y.-L. Chan, and Y.-J. Hsu, *J. Electron Spectrosc. Relat. Phenom.* **185**, 429 (2012).
- [33] G. E. Rhead, *J. Vac. Sci. Technol.* **13**, 603 (1976).
- [34] H. Lüth, *Surfaces and Interfaces of Solid Materials* (Springer, Berlin, 1995).
- [35] In the present work, the AES peaks of both Ni (MVV at 61 eV) and Co (MVV at 53 eV) are included as the signal of the Co/Ni underlayer.
- [36] F. Spaepen, *Acta Mater.* **48**, 31 (2000).
- [37] C. Kittel, *Introduction to Solid State Physics*, 8th ed. (John Wiley & Sons, New York, 2004).
- [38] K. Krupski, T. Kobiela, and A. Krupski, *Acta Phys. Pol. A* **125**, 1159 (2014).
- [39] C. Nagl, E. Platzgummer, O. Haller, M. Schmid, and P. Varga, *Surf. Sci.* **331-333**, 831 (1995).
- [40] H. L. Meyerheim, H. Zajonz, W. Moritz, and I. K. Robinson, *Sur. Sci.* **381**, L551 (1997).
- [41] M. Kabiruzzaman, R. Ahmed, T. Nakagawa, and S. Mizuno, *Sur. Sci.* **664**, 70 (2017).
- [42] T. Burkert, O. Eriksson, P. James, S. I. Simak, B. Johansson, and L. Nordström, *Phys. Rev. B* **69**, 104426 (2004).
- [43] L. Néel, C. R. Acad. Sci. **237**, 1468 (1953); *J. Phys. Radium* **15**, 225 (1954).
- [44] See Supplemental Material at <http://link.aps.org/supplemental/10.1103/PhysRevB.104.174407> for the information of the vertical interlayer distance, the calculation of the magnetic anisotropy energy of Pd, Pb, and Bi/Co/Ni films, and a comparison between the PMA and surface structure in wedge-shaped 0–3-ML Pb(Bi)/Co/Ni/Cu samples. Also see W. C. Lin, C. C. Kuo, C. L. Chiu, and M. T. Lin, *Surf. Sci.* **478**, 9 (2001); B. Schulz and K. Baberschke, *Phys. Rev. B* **50**, 13467 (1994); R. F. Willis, J. A. C. Bland, and W. Schwarzacher, *J. Appl. Phys.* **63**, 4051 (1988).
- [45] B. T. Thole, P. Carra, F. Sette, and G. van der Laan, *Phys. Rev. Lett.* **68**, 1943 (1992).
- [46] P. Carra, B. T. Thole, M. Altarelli, and X. Wang, *Phys. Rev. Lett.* **70**, 694 (1993).
- [47] R. Wu, D. Wang, and A. J. Freeman, *Phys. Rev. Lett.* **71**, 3581 (1993).
- [48] P. Bruno, *Phys. Rev. B* **39**, 865 (1989).
- [49] B. Y. Wang, J. Y. Hong, K. H. O. Yang, Y. L. Chan, D. H. Wei, H. J. Lin, and M. T. Lin, *Phys. Rev. Lett.* **110**, 117203 (2013).
- [50] The magnetocrystalline anisotropy of a FM layer is roughly proportional to the orbit/spin ratio in magnetic easy axis [21,48,49].
- [51] M. T. Johnsony, P. J. H. Bloemenz, F. J. A. den Broedery, and J. J. de Vries, *Rep. Prog. Phys.* **59**, 1409 (1996).
- [52] N. Nakajima, T. Koide, T. Shidara, H. Miyauchi, H. Fukutani, A. Fujimori, K. Iio, T. Katayama, M. Nývlt, and Y. Suzuki, *Phys. Rev. Lett.* **81**, 5229 (1998).
- [53] F. E. Gabaly, K. F. McCarty, A. K. Schmid, J. de la Figuera, M. C. Muñoz, L. Szunyogh, P. Weinberger, and S. Gallego, *New J. Phys.* **10**, 073024 (2008).